metals

MDPI

*Article*

# Fatigue Behavior Parametric Analysis of Dry Machined UNS A97075 Aluminum Alloy

**Sergio Martín Béjar, Francisco Javier Trujillo Vilches *, Carolina Bermudo Gamboa and Lorenzo Sevilla Hurtado**

Civil, Material and Manufacturing Engineering Department, EII, University of Malaga, Malaga 29071, Spain; smartinb@uma.es (S.M.B.); bgamboa@uma.es (C.B.G.); lsevilla@uma.es (L.S.H.)

* Correspondence: trujillov@uma.es; Tel.: +34-951952245

Received: 12 March 2020; Accepted: 11 May 2020; Published: 12 May 2020

**Abstract:** Fatigue behavior takes special relevance in structural parts for aircraft due to safety reasons. Despite its environmental advantages, dry machining of these parts may negatively affect their surface integrity, which may lead to a reduction in fatigue life. Nevertheless, there is a lack of research focused on the analysis of the cutting parameters influence on fatigue behavior in dry machining of aeronautical aluminum alloys, in spite of its importance. Therefore, in this work, an analysis of the cutting speed and feed influence on fatigue behavior of dry turned UNS A97075-T6 alloy is presented. The stress-fatigue life curves have been obtained and corrected according to the applied cutting parameters values. Additionally, the surface roughness and two macro-geometrical deviations (cylindricity and concentricity) have been controlled. The experimental results have revealed that fatigue life is reduced when high values of cutting speed and feed are combined. Finally, a parametric potential equation for fatigue life, as a function of the load and the cutting parameters, has been developed. The relation has been obtained for the theoretical fracture section and, as the main novelty, corrected for the real one.

**Keywords:** UNS A97075; dry machining; surface integrity; fatigue behavior; aluminum alloys; parametric equations

## 1. Introduction

Manufacturing processes global efficiency is related to four interconnected concepts: functional, energetic, environmental and economic performance [1,2]. Currently, one of the most important aspects to consider in manufacturing processes refers to their sustainability. This concept includes three important core ideas: economic, environmental and social impact. Hence, new manufacturing developments usually focus on the environment impact reduction and green production systems promotion. Nevertheless, the environmental performance improvement may result in functional, economic and energetic imbalances that should not be neglected [3,4]. In this regard, one of the industrial sectors that play a leading role in reducing environmental impact is the aeronautical industry, which is considered a strategic sector with highly special characteristics [5].

Light alloys, especially aluminum alloys (series 2000 (Al-Cu) and 7000 (Al-Zn)), have been traditionally used in the manufacturing of structural parts for aircrafts, due to their excellent weight/mechanical properties ratio [6,7]. Machining operations, among others, are commonly employed to manufacture these parts. Cutting fluids have been commonly used in these processes, in order to improve tool life and, as a result, the process economic performance. However, reducing (e.g., MQL, minimum quantity of lubricant techniques) or eliminating their use (dry machining) is the actual trend, because of their high toxicity and environmental harmful. Notwithstanding, the total absence of cutting fluids in machining operations generates severe conditions that may affect surface conditions of manufactured parts and, therefore, their performance in service [8–10].

Strong quality requirements are usually demanded in the manufacturing of structural parts for aircrafts, due to reliability and security reasons. In this sense, surface integrity becomes a very relevant quality property. Surface integrity can be defined as the set of material properties, exhibited, acquired or modified after any forming process. These properties can be considered from three points of view: micro-geometrical (surface profile, microcracks, etc.), macro-geometrical (cylindricity, concentricity, straightness, etc.) and physical-chemical and mechanical properties (microhardness, residual stresses, corrosion resistance, fatigue behavior, etc.) [11–15].

Among the different considered properties in the surface integrity, fatigue behavior takes special importance in the aeronautical industry due to safety reasons. Microcrack generation, nucleation and crack growth affect the in-service behavior of this type of structural component [16]. Therefore, fatigue behavior usually has a high dependence on the surface quality [17]. Consequently, a great attention should be paid to the design specifications and quality control of the machined parts surface. In this regard, three parameters are often proposed to evaluate surface influence on fatigue behavior: surface roughness, residual stresses and microstructure [18]. These parameters depend on the cutting conditions applied during machining operation and can vary separately.

The cutting parameters influence on surface roughness has been widely analyzed in the dry machining of aluminum alloys. Different research considers that the feed-rate ($f$) is the most influential cutting parameter on average roughness ($Ra$), regardless of the cutting speed ($v_c$) and the cutting depth ($a_p$) [19–23]. These studies have revealed that the feed-rate increment results in lower surface quality ($Ra$ increments). This fact may promote the microcrack appearance on the machined part surface and, consequently, may affect fatigue behavior.

Suraratchai et al. [18] considered the surface roughness of machined parts in terms of stress concentration, similar to a notch effect. A four-point bending fatigue test was carried out on different specimens of the UNS A97010 aluminum alloy. The specimens were machined in two directions (longitudinal and transversal), using cutting speed values of 12 and 50 m/min. The experimental results showed that lower surface roughness values resulted in better fatigue behavior. Notwithstanding, they concluded that the surface texture should not be considered as the predominant surface parameter, but residual stresses and microstructure should be also considered.

Wiesner et al. [24] evaluated the influence of UNS A97075 turned parts surface topography on fatigue life. Root mean square deviation ($Rq$) was the selected parameter to evaluate the surface quality. Different turning tests were performed with a feed-rate between 0.01 and 0.40 mm/rev, and 2 nose radius values, 0.40 and 0.80 mm. Furthermore, a heat treatment was carried out to eliminate the microhardness and residual stresses influence on fatigue behavior. Higher $f$ values and lower nose radius resulted in $Rq$ increments, which negatively affected fatigue behavior.

The residual stresses in machining can be both compressive (negative residual stress) and tensile (positive residual stress). Different research considers that the tool nose radius and the cutting parameters are related with the residual stresses generation [25–29]. The increase of the feed-rate tends to generate tensile residual stresses [29], whereas the decrease of the cutting speed tends to generate compressive stresses [28]. In addition, the cutting speed seems to be the most influential cutting parameter on residual stresses. Notwithstanding, the residual stresses sign depends on the combination of both cutting parameters, $v_c$ and $f$. In this regard, several studies consider that the tensile residual stresses result in fatigue strength reduction, whereas the compressive residual stresses improve it [30–32]. Therefore, different cutting parameters combinations may affect positively or negatively the material fatigue behavior of machined parts.

Nose radius and feed-rate influence on the fatigue behavior of 34CrNiMo6 alloy was studied by Javidi et al. in [33]. The experimental results showed that higher $f$ values and lower nose radius results in a fatigue life increase, due to an increase of the compressive residual stresses, caused during machining process.

Sun et al. in [34] studied the cutting speed influence on turning operations of nickel alloy GH4169. The specimens were tested at 15, 30 and 45 m/min. In this case, the cutting speed value of 30 m/min showed the highest compressive residual stress and, as a result, the best fatigue behavior.

Gómez Parra in [35] studied the influence of $f$ (0.05 and 0.20 mm/rev) and $v_c$ (120, 170 and 200 m/min) on residual stresses of the UNS A92024 alloy, turned under dry conditions. On one hand, the residual stresses were analyzed at different depths from the surface (up to 1 mm deep). In the surface proximity (less than 0.2 mm), tensile residual stresses were observed. Nevertheless, compressive residual stresses were obtained for deeper values. In this case, higher $v_c$ and lower $f$ exhibited a general trend to produce higher compressive residual stresses. In addition, $v_c$ was the most influential cutting parameter on the residual stresses behavior. On the other hand, the influence of cutting parameters on fatigue behavior was also analyzed. The research concluded that feed-rate was the most relevant cutting parameter. A fatigue life reduction was observed when the feed-rate was increased. The cutting speed influence was only significant for the low range of the feed-rate studied. For this range, a fatigue life decrement was observed for the cutting speed highest values.

Surya et al. in [36] analyzed the influence of $v_c$ and $a_p$ on residual stresses of turned parts of the UNS A97075 alloy. The tests were conducted under different values of $v_c$ (50, 100, 200 and 300 m/min) and $a_p$ (0.3, 0.6 and 0.9 mm). A constant feed-rate was considered, $f$ (0.05 mm/rev). The results revealed that the residual stresses on the surface of machined parts were tensile. In a range of 50–200 m/min, the tensile stresses increased with $v_c$, whereas these residual stresses decreased for higher values of $v_c$ (300 m/min). Furthermore, the $a_p$ increase resulted in tensile stresses increments. Notwithstanding, $v_c$ was the most influential cutting parameter.

In addition, machining operations modify surface metals microstructure due to plastic strain, grain growth, strain hardening and phase change [37]. The influence of surface microstructure on fatigue behavior can be evaluated by a surface microhardness test. A microhardness increase makes the microcracks appearance in the surface less likely.

Surya et al. in [36] additionally evaluated the influence of $v_c$ and $a_p$ on surface microhardness. The increase of both cutting parameters resulted in a decrease of surface microhardness due to the heat dissipation during machining operation. Additionally, the authors concluded that $v_c$ was the most influential parameter. These results are in good agreement with those obtained by Campbell et al. in [38].

Finally, the microstructure change due to machining operations reaches a depth range between 50 and 500 μm [38,39]. In this range, microcrack generation and nucleation takes place. Hence, the microstructure grain may affect fatigue behavior.

Considering the aforementioned research, the surface condition can be related to fatigue behavior in different materials. This surface condition strongly depends on cutting parameters [19,40,41], especially in dry machining [42–44]. Despite its importance, the effects of these variables (surface roughness, residual stresses and microstructure) on fatigue behavior are commonly accounted using empirical reduction factors, modifying the material strength limit or fatigue life [45]. Furthermore, most of the research focuses on the analysis of cutting parameters influence on several output variables of the process (residual stresses, surface roughness and microstructure), usually separately. These variables have different trends depending on the cutting parameters, which affect fatigue behavior in different ways. In addition, the measurement of these variables usually requires very complex measurement systems (normally offline). However, there is a lack of research that focuses on the analysis of the cutting parameters influence on fatigue behavior, especially in the dry machining of light alloys, aluminum alloys among them. This may be due to the large number of tests to be performed, because of the large dispersion in the results that this kind of fatigue life test normally exhibits.

Therefore, surface integrity includes aspects related to geometry, mechanical and physical-chemical properties on the surface. Geometric aspects include deviations at a microscale (roughness profile) and macroscale (dimensional tolerances and geometric deviations: straightness, roundness, cylindricity, concentricity, etc.). The analysis of the cutting parameters influence on variables such as surface roughness, residual stresses or the microstructure have already been addressed by other researchers, as well as the influence of these output variables on the fatigue behavior. However, the analysis of the geometrical deviations on fatigue behavior has not been

analyzed yet. In addition, the direct relationship between cutting parameters and fatigue behavior has not been carried out either. This kind of analysis is highly demanded by the manufacturing industry, because it usually provides easy-to-apply equations that allow predicting the behavior of the process output variable based only on the input parameters.

Therefore, in this work, an analysis of the cutting speed and feed-rate influence on fatigue behavior of the UNS A97075-T6 alloy, machined under dry conditions, is presented. The analysis has been performed according to the ISO 1143:2010 standard (metallic materials—rotating bar bending fatigue testing) [46]. The tests have been carried out for different loads and cutting parameters combinations, in order to obtain the Wöhler curve for this material, corrected according to the cutting parameters applied. Additionally, the surface profile and different macro-geometrical deviations (cylindricity and concentricity) have been evaluated in the calibrated area of the specimens, in order to control their possible influence on fatigue behavior. Finally, a parametric potential equation for fatigue life is proposed. This relation allows predicting the fatigue life as a function of the stress in the fracture section and the applied cutting parameters values. The equation has been developed for the theoretical fracture section and it has been corrected for the real one.

## 2. Materials and Methods

The material selected for this research was the UNS A97075-T6 aluminum alloy, commonly used in the aeronautical industry to manufacture structural parts (such as wings, fuselage and the aircraft tail) [47]. The composition of the tested alloy is shown in Table 1, obtained by arc atomic emission spectroscopy (AES).

**Table 1.** UNS A97075-T6 composition (mass %).

| Zn | Mg | Cu | Cr | Si | Mn | Al |
|---|---|---|---|---|---|---|
| 6.03 | 2.62 | 1.87 | 0.19 | 0.09 | 0.07 | Rest |

Different standards allow one to evaluate the fatigue behavior of metallic materials, Table 2 [46,48–50]. For this research, the standard ISO 1143:2010 "Metallic materials – rotating bar bending fatigue testing" has been selected, due to several reasons: implementation ease; the test duration can be reduced by increasing the rotational speed of the test bench; aeronautical parts are usually subjected to bending stresses [51,52] and equipment availability.

**Table 2.** Fatigue test and associated standards.

| Fatigue test behavior | Standard |
|---|---|
| Rotating bar bending test | ISO 1143:2010 |
| Axial force controlled method | ISO 1099:2006 |
| Axial strain controlled method | ISO 12106:2003 |
| Torque controlled fatigue testing | ISO 1352:2011 |

A rotating bar bending equipment was used to perform the fatigue test. This equipment was designed and manufactured according to the ISO 1143:2010 standard [46], in the University of Malaga, by reusing the kinematic chain of an old parallel lathe that was out of service [53]. The equipment allows applying a single-point load in the extreme of the specimen, Figure 1a. The specimen geometry and dimensions are shown in Figure 1b.

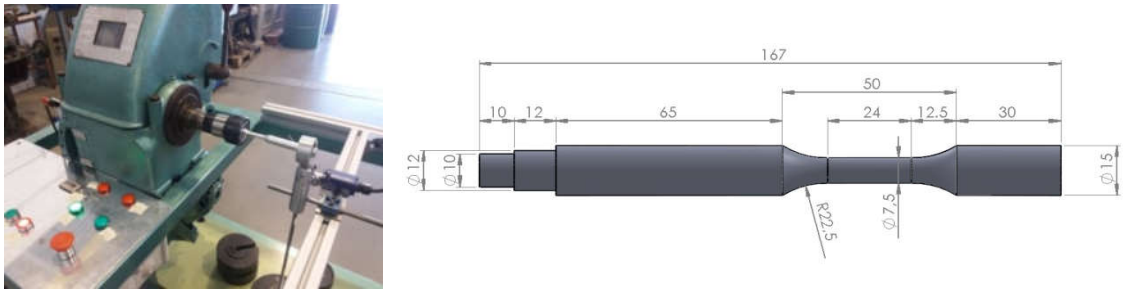


(**a**) (**b**)

**Figure 1.** (**a**) Fatigue test bench and (**b**) specimen geometry and dimensions (mm).

*2.1. Machining Test*

Different machining tests were carried out in a turning center. All the tests were performed under dry conditions in order to use friendly environmental techniques and thermal treatments were not used on machined parts to preserve their surface conditions. Extruded bars were used, coming from a single batch. A scanning electron microscopy (SEM) analysis was performed to guarantee microstructure homogeneity in the extrusion main direction. These bars were subjected to roughing machining operations (performed under the same cutting conditions) up to the specimen dimensions before the finishing operation. This guarantees starting the tests in the most homogeneous conditions as possible. This finishing operation was the object of study, modifying the different cutting parameter values.

The selected cutting tool and its configuration were the usual in the turning of this alloy and compatible with the specimen geometry to be machined. A rhombic uncoated WC-Co tool (ISO DCMT 11T308-14 IC20) was used in a neutral position during the turning operation. A new cutting edge has been used for each test in order to ensure the same initial conditions.

For the finishing operation, different cutting parameter combinations were selected to evaluate their influence on fatigue behavior. Table 3 shows the cutting speed ($v_c$) and the feed-rate ($f$) selected values. Due to the large amount of test to be performed, the cutting depth ($a_p$) remained constant. In this regard, it is necessary to highlight that previous research has revealed that $a_p$ is the cutting parameter with less influence on surface condition [54], in the dry turning of this alloy. Additionally, the cutting speed and the feed-rate are more relevant in other output variables that affect fatigue behavior, such as residual stresses, microhardness and surface microstructure [25,28,29,33].

**Table 3.** Cutting parameters.

| $v_c$ (m/min) | $f$ (mm/rev) | $a_p$ (mm) |
|---|---|---|
| 40 | 0.05 | 1.0 |
| 60 | 0.10 | |
| 80 | 0.15 | |
| | 0.20 | |

The selected values for the cutting parameters are commonly used in the machining of these alloys for particular aeronautical applications. In addition, these cutting conditions were selected in order to compare the results of this study with previous related works [55,56]. In this context, it should be pointed that although low cutting speed is not recommended for machining aluminum alloys, these alloys are often used hybridized with other materials, such as carbon fiber reinforced polymers (CFRP) to form fiber metal laminates (FML), in which this low cutting speed is required. In addition, these low cutting speed values are compatible with the low diameter values required in the standard, in order to maintain a reasonable spindle speed [10,33,35].

Twelve Wöhler curves have been obtained (corresponding to each of the 12 possible combinations of cutting parameters). Those 12 Wöhler curves were determined by 4 points (corresponding to each of the four loads). Four repetitions for each test were carried out for each

cutting parameter combination, according to the ISO 12107:2012 standard [57], to ensure the repeatability of the tests (95% confidence level and a 50% failure probability). Therefore, 4 loads, 12 cutting parameter combinations and 4 repetitions were carried out (192 specimens tested).

After the turning test was performed, a geometrical control was carried out to ensure that the specimens were manufactured according to the design dimensions. The diameter was controlled with an outside micrometer (scale division = 0.001 mm). Additionally, the micro-geometrical deviations were controlled. The average roughness (*Ra*) was used as the characteristic parameter of the roughness profile. A roughness tester (Mitutoyo SJ-210) was used to obtain the roughness profile. Different measurements were carried out along four generatrix of the specimen (90° apart). The *Ra* value was expressed as the average of the different performed measurements.

Finally, the specimen concentricity and cylindricity were controlled using an online method. These geometrical deviations were obtained by the measurement of the roundness and the circular runout in six sections of the calibrated area, separated 4 mm from each other, using a millesimal dial gauge with a measuring range of 12.5 mm, scale division of 0.001 mm and a maximum permissible error (MPE) of 4 μm (Figure 2a). The experimental setup was validated using a geometrical deviation measurement machine (offline method), Figure 2b. The differences were less than 10%.

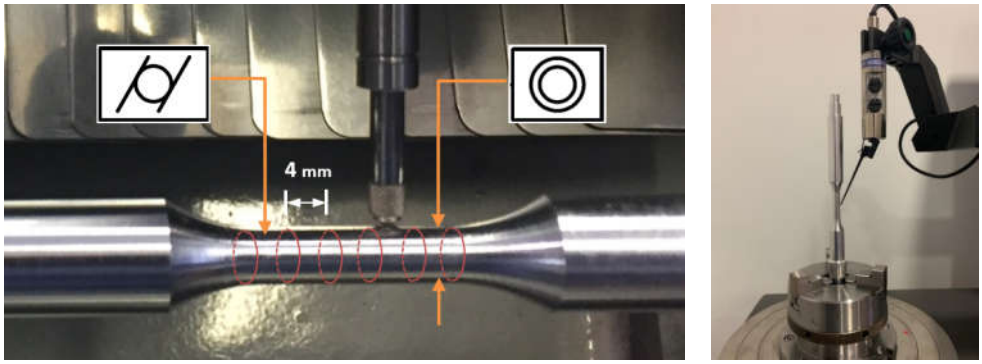


(**a**) (**b**)

**Figure 2.** (**a**) Concentricity and cylindricity control in the calibrated area and (**b**) experimental setup validation in a geometrical deviation measurement machine.

Four different loads (Table 4) were applied in order to get the Wöhler curve, which relates the fatigue life (number of cycles, *N)* versus the stress (*S*). Therefore, 192 specimens were tested in this work. Taking into account the load applied, the mass of the element that supports the load (0.54 kg), and the geometry of the specimen (Figure 1b), Equation (1) allows calculating the bending stress applied in the expected fracture section.

$$S = \frac{32 \cdot F \cdot (L - x)}{\pi \cdot d^3}, \quad (1)$$

where the different variables correspond to (Figure 3):

- *S*: Stress in the fracture section (MPa);
- *L*: distance between the load applied section and the fixed test point (mm);
- *x*: distance between the fixed test point and the maximum stress point (mm);
- *d*: calibrated zone diameter (mm);
- *F*: Load and support load applied in the test (*N*).

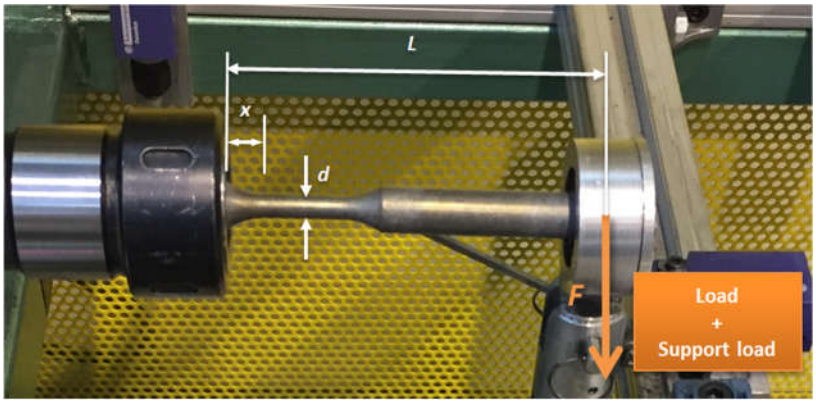


**Figure 3.** Variables to calculate the stress in the fracture section.

In this work, the values for the different parameters in Equation (1) were: $L$ = 121 mm, $x$ = 12.5 mm and $d$ = 7.5 mm. Table 4 shows the fracture section stress as a function of the applied loads and the support load (fixed for each test).

**Table 4.** Fracture section stress as a function of the applied loads.

| Load (N) | Support Load (N) | Stress (MPa) |
|---|---|---|
| 88.20 | 5.10 | 244.40 |
| 93.10 | | 257.24 |
| 98.00 | | 270.08 |
| 102.90 | | 282.91 |

Once the specimen was placed in the fatigue test bench and before starting the test, the concentricity between the extreme of the specimen and the chuck was controlled (Figure 4a), according to the ISO 1143:2010 standard [46]. In order to do that, 2 dial gauges were used to take geometrical deviations each 30°. The concentricity was lower than that required by the standard in all cases. Furthermore, during the test, a temperature control was performed with a thermographic camera (Figure 4b), remaining the temperature of the test around 23 °C. Hence, the limit temperature (35 °C) established by the standard (ISO 1143:2010) was not exceeded in any test. Below this limit the standard indicates that it is not necessary to take into account the temperature effect and its effect on fatigue behavior can be considered negligible. The tests were carried out at a rotational speed of 2800 rev/min. The number of cycles ($N$) was registered once the specimen fractured.

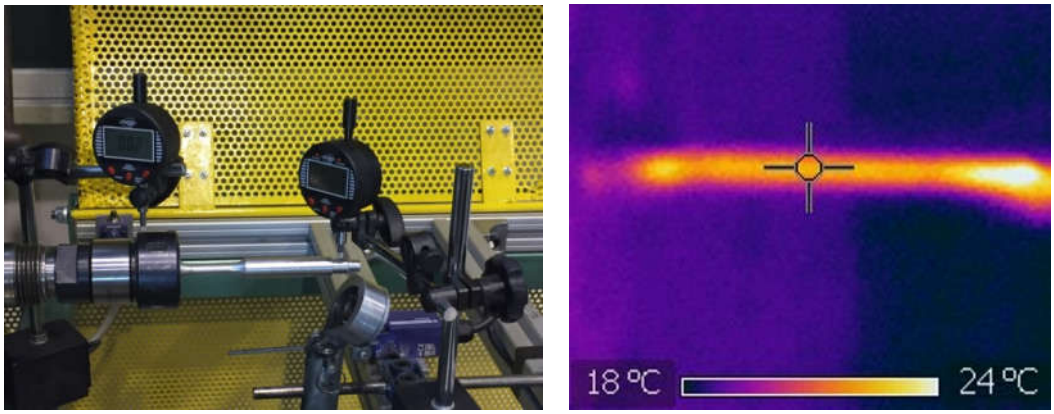


(**a**) (**b**)

**Figure 4.** Rotating bar bending test control: (**a**) concentricity control setup before starting the test and (**b**) specimen temperature during the test.

Finally, a fractography analysis of the fracture sections was performed to ensure the correct fatigue fracture procedure. The fracture section was off-line monitored by using stereoscopic optical microscopy (SOM) techniques. For this purpose, a stereoscopic microscope NIKON, SMZ 2T model, with a Kappa Image Base CF11 DSP camera and a PCI SC module capture card was used. Figure 5a shows an image of a fracture section (13×) and Figure 5b focuses on the fatigue initial crack (30×).

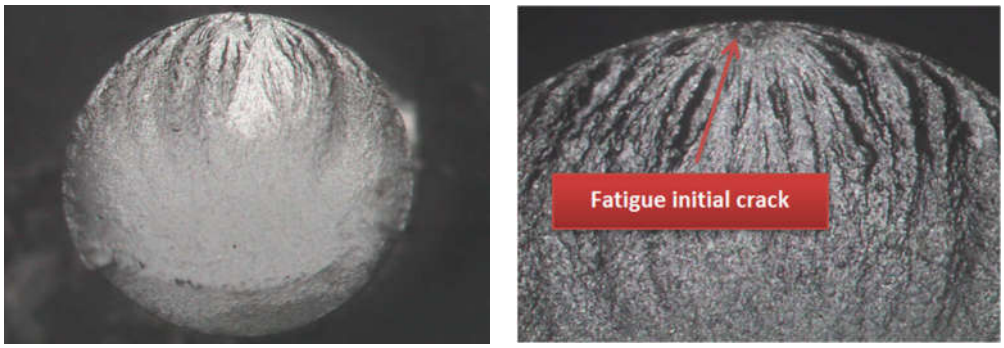


(**a**) (**b**)

**Figure 5.** Fractography test: (**a**) fracture section (13×) and (**b**) fatigue initial crack (30×).

It is important to highlight that with SOM images, the fatigue initial crack, the crack growth and the final fracture surfaces can be observed [39]. In spite of this, a deep fracture section analysis requires scanning electron microscopy (SEM). However, it was not carried out due to it not being the main objective of this work.

## 3. Results and Discussion

As indicated in the methodology section, several quality controls were carried out at macro-geometric (diameter and form deviations) and micro-geometric (roughness profile) scales, according to the ISO 1143:2010 standard. Regarding the diameter of the calibrated area, all the experimental values were within the standard requirements (d ± 0.02 mm). The experimental results for the surface roughness and the fatigue behavior are reported below, as well as a summary of the form deviations, widely analyzed in previous works [56].

### *3.1. Surface Roughness*

Figure 6 shows the average experimental results for *Ra* as a function of $v_c$ and *f*. A general trend to increase *Ra* with *f* was observed, regardless of $v_c$. The best result was obtained for the lowest feed value (0.05 mm/rev), close to the reference surface roughness obtained by polishing with a fluid, for this kind of aluminum alloy. A slight increase of *Ra* was observed when *f* increased from 0.05 to 0.10 mm/rev. Nevertheless, this growth was more noticeable from 0.10 to 0.20 mm/rev. The *Ra* highest values were obtained for 0.20 mm/rev, regardless $v_c$.

Regarding the cutting speed, its influence on *Ra* was less noticeable. It was observed that at low feed (0.05–0.10 mm/rev) the cutting speed influence on both the mean value and the dispersion was lower. For the high range of feed (0.15–0.20 mm/rev) the cutting speed influenced results in a greater dispersion in the roughness values, being more noticeable at 0.15 mm/rev for the roughness average values.

Therefore, *Ra* strongly depended on *f*, being this cutting parameter the most influential on micro-geometrical deviations, in good agreement with previous research [18,24].

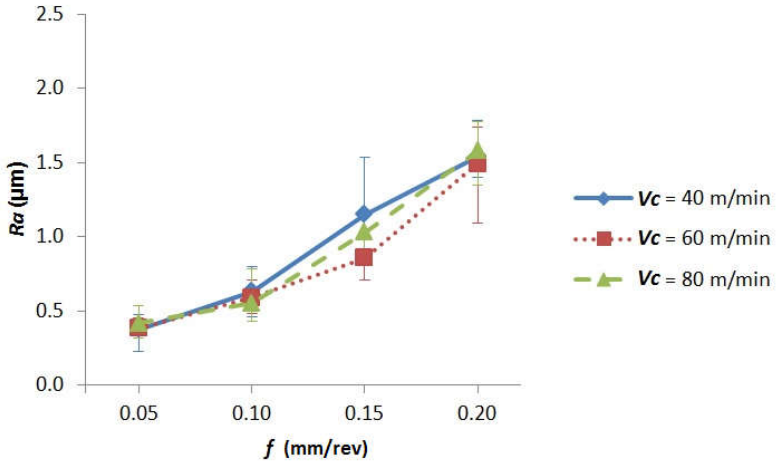


**Figure 6.** Surface roughness (*Ra*) in the function of $v_c$ and *f*.

### 3.2. Fractography

The specimens were analyzed after the fatigue testing, employing SOM techniques, in order to characterize the fatigue fracture surfaces. Such characterizations involve the identification of the crack initiation areas, the crack growth and ductile fracture zone in the fatigue fracture mechanism (Figure 7).

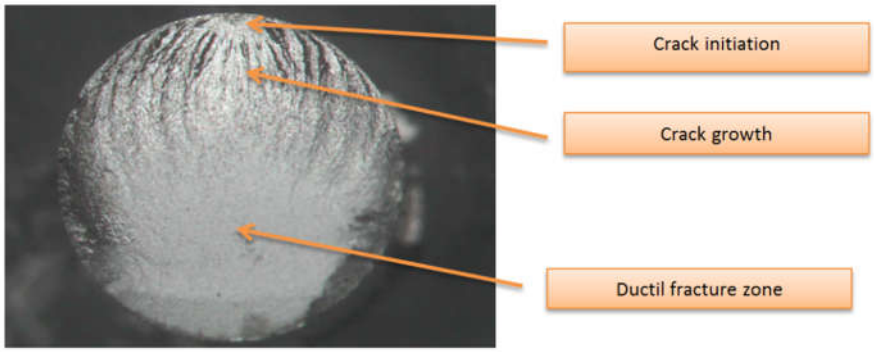


**Figure 7.** Fatigue fracture surface characterization (13×).

Figure 8 shows an example of the fracture surface of several specimens, which were tested with different loads. Figure 8 represents only one of the possible combinations of cutting parameters, but it is representative of the other combinations. These specimens were turned with $v_c$ = 80 m/min and *f* = 0.20 mm/rev. As it can be observed, the features of the fracture surface of the specimens were very similar, regardless of *S*, with the exception of the ductile fracture zone size, which seems to be smaller at higher alternating stress, as expected. It is necessary to highlight that these observations were valid within the range of *S* values tested.

All cases analyzed show that crack initiation appeared in a point of the surface specimen. Different curve bands on the crack growth surface, corresponding with surface waves, were clearly observed. This effect can be considerate due to the fatigue failure that occurred as a transgranular propagation of the fatigue crack [58]. Thus, the cutting parameters did not affect the features of the fracture surface, being *S* the most influential parameter.

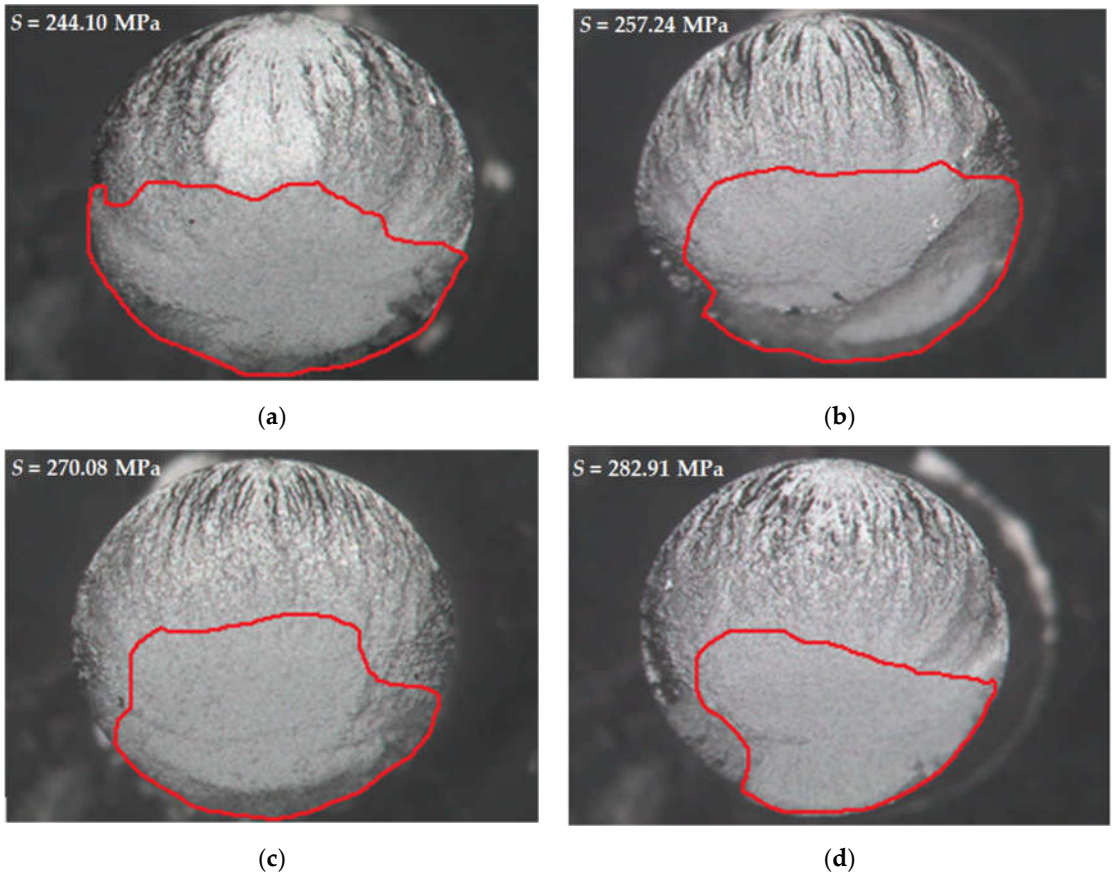


**Figure 8.** SOM images of the fatigue fracture surface (13×): (**a**) $S$ = 244.10 MPa; (**b**) $S$ = 257.24 MPa; (**c**) $S$ = 270.08 MPa and (**d**) $S$ = 282.91 MPa.

### *3.3. Fatigue Behavior Parametric Analylsis*

Figure 9 shows the evolution of $N$ as a function of $v_c$ and $f$, for each applied load. Regarding $f$, a general trend to decrease $N$ with $f$ was observed, regardless of $v_c$. This trend was more evident within the low range of load applied (244.40 and 257.24 MPa). Therefore, the surface topography was especially relevant in the crack initiation of fatigue failure at lower stresses and, as a result, $f$ becomes more regardless. At higher stresses, this influence became lower and, therefore, surface roughness became less relevant. At high loads, other factors may be more prominent, such as the geometrical deviations, residual stresses or microstructure, which are more influenced by the cutting speed [56]. Notwithstanding, some singularities in this trend are observed for the low range of $f$ applied (0.05–0.01 mm/rev), for $v_c$ = 40 and 60 m/min, where a reduction of $N$ was observed for some of the loads studied. This can be explained taking into account that the highest dispersion occurs for these $v_c$ values. Under these cutting conditions, the distance between the real and expected fracture section was also the highest.

With regard to $v_c$, a general trend to decrease $N$ with $v_c$ was observed, regardless of $f$. Only for $v_c$ = 60 m/min this trend was the opposite within the low range of $f$ (0.05–0.10 mm/rev) and $S$ (244.40 and 257.24 MPa). In addition, the worst results were obtained when the highest $f$ and $v_c$ were combined. Furthermore, in Figure 9c, for $v_c$ = 40 m/min and $f$ = 0.10 mm/rev, the increase of $N$ could be explained because the distance between the expected fracture section and the real one was higher, reducing the equivalent stress and increasing $N$.

Additionally, the increase of $S$ (in connection with the load increase) gave rise to a reduction of $N$ in the whole range of the cutting parameters values, as expected. However, the effect of the applied cutting parameters in the machining process should not be neglected. For each tested value of $S$, $v_c$ and $f$ have modified the fatigue behavior of the turned parts. In general, they have negatively

affected the fatigue behavior, reducing $N$. On one hand, an $f$ increment results in higher $Ra$ values, which makes easier the crack initiation. On the other hand, a $v_c$ increase gives rise to a microhardness reduction, an increment of geometrical deviations (due to higher vibrations) and an increase of tensile stresses [36,55,56], which results in $N$ reductions. Those effects are enhanced when both cutting parameters ($f$ and $v_c$) increase simultaneously.

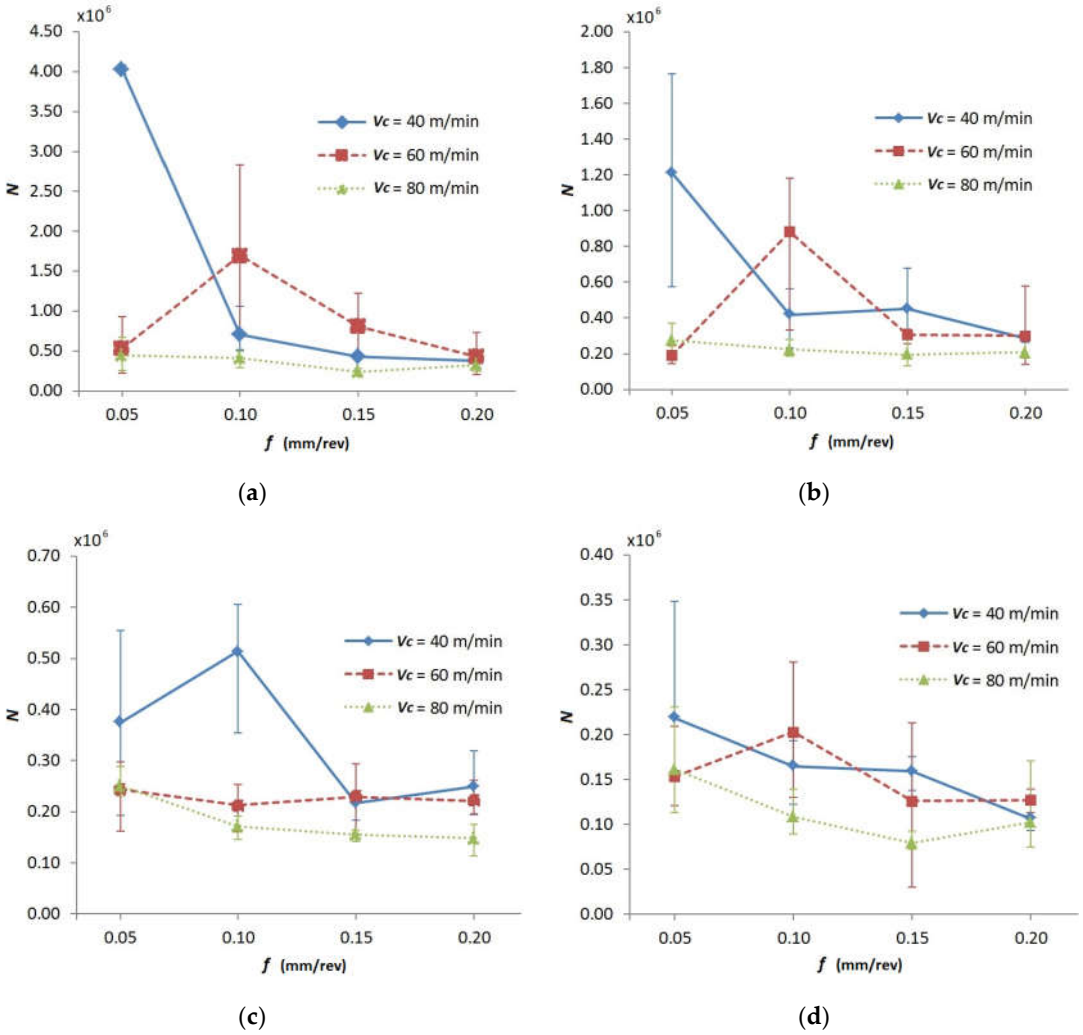


**Figure 9.** Number of cycles ($N$) as a function of $v_c$ and $f$, for different $S$ values: (**a**) 244.40 MPa; (**b**) 257.24 MPa; (**c**) 270.08 MPa and (**d**) 282.91 MPa.

These experimental results suggest the possibility of obtaining an equation that relates fatigue life not only with the stress (or the load) but also with the cutting parameters.

First, the relation $S$-$N$ (Basquin's equation) has been obtained for each cutting parameters combination. For this marginal equation the cutting speed and feed have remained constant. A potential relation, as shown in Equation (2), is usually used [39]. This equation allows obtaining a relation between $S$ and $N$.

$$S = C \cdot N^{\alpha}, \tag{2}$$

In Equation (2), C and α are constant. This type of potential equations can be fit from the experimental data using a linear regression (log-log). Table 5 shows the results for these constants, according to ISO 12107:2012 [57]. These parametric relationships show, in general terms, a

reasonable fit ($R^2$ = 0.7–0.8) for most cutting parameters combinations, taking into account the usual dispersion of fatigue test results.

For an easier understanding, results are shown as *S-log N* (Wöhler curve) for each cutting parameter combination considered (Figure 10).

**Table 5.** *S-N* potential equation results.

| $v_c$ (m/min) | $f$ (mm/rev) | Equation Coefficients | | |
|---|---|---|---|---|
| | | C | α | $R^2$ |
| 40 | 0.05 | 474.55 | −0.043 | 0.87 |
| | 0.10 | 633.80 | −0.068 | 0.58 |
| | 0.15 | 910.49 | −0.099 | 0.77 |
| | 0.20 | 882.05 | −0.098 | 0.78 |
| 60 | 0.05 | 574.64 | −0.063 | 0.42 |
| | 0.10 | 502.37 | −0.050 | 0.75 |
| | 0.15 | 522.37 | −0.055 | 0.72 |
| | 0.20 | 634.84 | −0.071 | 0.50 |
| 80 | 0.05 | 785.13 | −0.088 | 0.54 |
| | 0.10 | 903.65 | −0.101 | 0.87 |
| | 0.15 | 904.59 | −0.103 | 0.74 |
| | 0.20 | 853.76 | −0.097 | 0.80 |

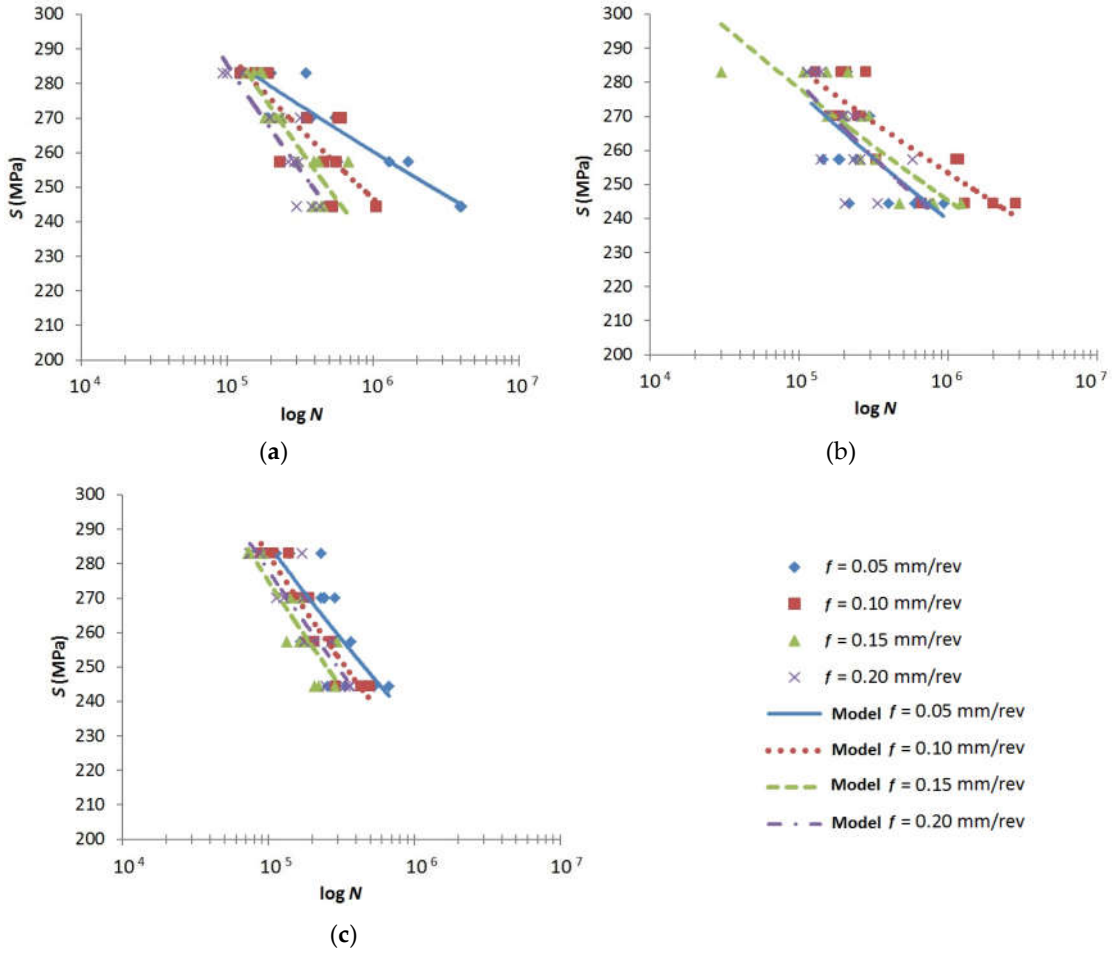


**Figure 10.** *S-N* parametric relationships vs. experimental data: (**a**) $v_c$ = 40 m/min; (**b**) $v_c$ = 60 m/min and (**c**) $v_c$ = 80 m/min.

On one hand, for $v_c$ = 40 m/min (Figure 10a), the results revealed a clear influence of *f* in the *S-N* relation, where an increase of *f* tended to reduce the *N* values, regardless of *S*. This fact is more noticeable for the lowest *S* (244.40 MPa), where the highest difference for *N* was obtained. In this regard, higher differences in the fatigue life (*N*) were observed for low *f* values (0.05–0.10 mm/rev) whereas these differences were lower for higher values (0.15–0.20 mm/rev). These differences became less relevant when *S* increased and *N* tended to converge to the highest *S* (282.91 MPa). In that point, *N* exhibited less sensitivity to change with *f*. This fact was in good agreement with that mentioned above. For lower *S* values, the surface conditions took more relevance. Higher *f* resulted in higher *Ra* (worse surface quality), which makes easier microcrack generation and nucleation [59]. However, crack initiation occurred faster for higher values of *S* and surface topography became less relevant.

On the other hand, for $v_c$ = 60 m/min (Figure 10b), a lower *f* influence on the *S-N* relation was observed. In general, as with $v_c$ = 40 m/min, a higher *f* influence could be observed at low *S* values (244.40 MPa), tending to converge at higher *S* values (282.91 MPa). Notwithstanding, the worst results were obtained for *f* = 0.05 mm/rev. Hence, *f* became less predominant and $v_c$ took more relevance. In addition, although the dispersion was greater for $v_c$ = 60 m/min, it is within the common dispersion for fatigue tests. Similar studies carried out on the cutting parameters influence on the microhardness and microstructure of the machined surface (which affect fatigue behavior) coincide in obtaining a greater dispersion in the results for $v_c$ = 60 m/min [55]. The authors explain this behavior due to a combined effect of mechanical effects (feed) and thermal effects (cutting speed) that influences on surface microhardness and microstructure and, therefore, on fatigue behavior.

Finally, for $v_c$ = 80 m/min (Figure 10c), the proposed equations and the experimental results, seemed to remain parallel along the whole *S* range. Additionally, in this case, the worst results were obtained for *f* = 0.15 mm/rev.

Considering that $v_c$ had a very low influence on *Ra*, everything seemed to indicate that other variables (not only micro-geometrical deviations) took parts in the *S-N* evolution, especially for higher values of $v_c$ (60–80 m/min). As previously mentioned, different research establishes that fatigue behavior is related with other surface conditions, as residual stresses, microstructure and surface microhardness [36,38], which are more influenced by $v_c$. This fact is relevant enough because, traditionally, Wöhler curves are corrected only as a function of the micro-geometrical surface deviations [59] and, hence, the effect of $v_c$ is usually neglected.

Since experimental data have revealed the influence of both cutting parameters on the fatigue life of the specimens, it is reasonable to modify the *S-N* relation as a function of $v_c$ and *f*. In the present work, obtaining a relationship of the studied output variable (fatigue behavior) as a function of the input variables (load and cutting parameters) may be interesting. Therefore, a new equation is proposed as an adaptation of the Basquin's equation that may be useful from an industrial point of view. Initially, different marginal equations ($v_c$ constant) that relate *N* with *S* and *f* have been developed, Equation (3).

$$N = C \cdot S^x \cdot f^y, \tag{3}$$

In Equation (3), C, x and y are constants. Table 6 shows the results for these constants. The exponent for *f* (*y*) shows higher value for $v_c$ = 40 m/min, which highlights the *f* greater influence on *N* at low cutting speeds. At higher cutting speed, *y* takes a lower value, the *f* influence being practically negligible for $v_c$ = 60 m/min. These results were in good agreement with the experimental data. In addition, the equations show a reasonable fit, considering the usual dispersion in the fatigue test results, due to the synergistic action of different factors, such as surface roughness, geometric deviations, residual stresses, surface microstructure changes or vibrations [39,60].

**Table 6.** Values of the constants for the marginal equation, $N = h(S,f)$.

| $v_c$ (m/min) | *C* | *x* | *y* | $R^2$ |
|---|---|---|---|---|
| 40 | $3.66 \cdot 10^{31}$ | −11.09 | −0.90 | 0.79 |

| | | | | |
|---|---|---|---|---|
| 60 | $4.92 \cdot 10^{31}$ | −10.83 | −0.03 | 0.63 |
| 80 | $1.82 \cdot 10^{23}$ | −7.55 | −0.34 | 0.91 |

Finally, potential parametric relationships, $N = g(S, v_c, f)$, have been proposed, which includes the effect of $v_c$, as follows (Equation (4)).

$$N = C \cdot S^{x} \cdot v_c^{z} \cdot f^{y}, \quad (4)$$

In Equation (4), C, x, y and z are constants. Table 7 shows the results for these constants. It is observed that *z* shows higher value than *y* (more than double). Therefore, the equation reveals that $v_c$ has higher relevance than *f* in the fatigue life (*N*). In addition, both exponents are negative and, therefore, $v_c$ and *f* tend to reduce the fatigue life of the specimens.

**Table 7.** Values of the constants for the equation, $N = g(S, v_c, f)$.

| C | x | z | y | $R^2$ |
|---|---|---|---|---|
| $2.89 \times 10^{30}$ | −9.83 | −0.92 | −0.42 | 0.71 |

The results from Table 7 revealed that Equation (4) has shown a reasonable fit ($R^2 = 0.71$) within a wide range of cutting speed, regardless of *f*, taking into account the normal dispersion of fatigue tests. For $v_c = 40$ m/min, this equation allows one to get a good approximation for *N*, as it could be observed for the marginal equations from Table 6 ($R^2 = 0.79$), being higher for $v_c = 80$ m/min ($R^2 = 0.91$).

However, for $v_c = 60$ m/min, the equation fit shows a lower value ($R^2 = 0.63$). For this cutting speed the dispersion of experimental results was greater but, as previously commented, within the common dispersion for fatigue tests. In fact, for this $v_c$ value (60 m/min), the combination of the thermal and mechanical effect (cutting speed and feed, respectively) gave rise to singularities in the microhardness and microstructure of the machined surface (which affect fatigue behavior) [55]. Regardless of the fit value, this equation allows for explaining the relative importance of each cutting parameter on *N*.

As previously mentioned, this relation indicates that surface roughness was not the only variable that affected fatigue behavior, but other variables, such as residual stresses, microhardness and surface microstructure, should be considered. Furthermore, this equation highlights the importance of the cutting parameters ($v_c$, *f*), especially when high $v_c$ and *f* values are combined.

### *3.4. Effect of the Real Fracture Section Position on Fatigue Behaviour*

ISO 1143:2010 standard demands strong requirements for geometrical tolerances of the rotating bar bending specimen, in order to minimize their effect in fatigue behavior. In this regard, the standard establishes maximum geometrical deviations values for roughness ($Ra < 0.32$ μm), concentricity ($CON < 15$ μm) and cylindricity ($CYL < 20$ μm). In addition, due to economic reasons, industrial machining operations use cutting conditions that can result in higher geometrical deviations. Therefore, both micro and macro-geometrical deviations influence should be considered in the fatigue behavior analysis. In order to do this, concentricity and cylindricity were measured before the fatigue tests. Table 8 shows the average values for the micro and macro-geometrical deviations.

**Table 8.** Geometrical deviations of the fatigue test specimens.

| $v_c$ (m/min) | *f* (mm/rev) | *Ra* (μm) | *CON* (μm) | *CYL* (μm) |
|---|---|---|---|---|
| 40 | 0.05 | 0.38 | 5.05 | 19.41 |
| | 0.10 | 0.63 | 6.86 | 35.09 |
| | 0.15 | 1.15 | 8.14 | 48.19 |
| | 0.20 | 1.54 | 15.92 | 41.64 |
| 60 | 0.05 | 0.38 | 5.55 | 12.19 |
| | 0.10 | 0.59 | 8.56 | 49.98 |
| | 0.15 | 0.86 | 9.82 | 20.93 |

| | | | | |
|---|---|---|---|---|
| | 0.20 | 1.49 | 24.54 | 90.96 |
| 80 | 0.05 | 0.42 | 3.63 | 31.74 |
| | 0.10 | 0.55 | 7.53 | 40.23 |
| | 0.15 | 1.03 | 31.18 | 62.86 |
| | 0.20 | 1.58 | 45.83 | 94.21 |

As it can be observed in Table 8, *Ra* values were higher than the standard requirements in the whole range of cutting parameters tested. Similar behavior could be observed in *CYL*, except for low *f* (0.05 mm/rev) and $v_c$ (40 and 60 m/min). On the other hand, *CON* seemed to be lower than standard requirements, except for the highest value of $v_c$ (80 m/min). Hence, these macro-geometrical deviations may be an important factor to consider, mainly in the high range of the applied cutting parameters values. These high values for the macro-geometrical deviations may result in the specimen fracture in a different area from that expected (maximum stress), Figure 11.


**Figure 11.** Rotating bar bending test fractured.

Hence, in this work, as a novelty, different stress values were calculated (Equation (1)), as a function of the real position where a fracture occurs. These stress values were related to the number of cycles (*N*), giving rise to new experimental Wöhler curves, Figure 12.

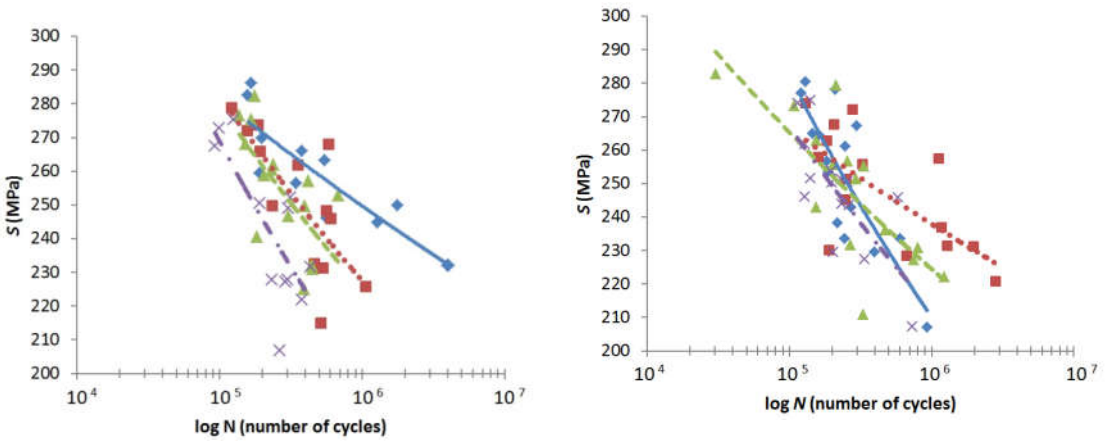


(**a**) (**b**)

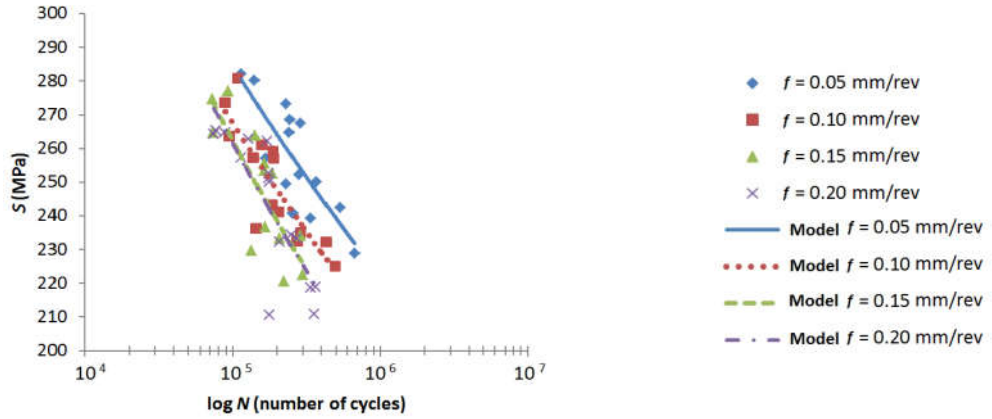


(**c**)

**Figure 12.** *S-N* parametric relationships vs experimental data, for the stress in the real fracture section: (**a**) $v_c$ = 40 m/min; (**b**) $v_c$ = 60 m/min and (**c**) $v_c$ = 80 m/min.

As a result, new potential relationships were developed. Table 9 shows the values of the constants for the new *S-N* potential equation, as a function of *f* and $v_c$, according to Equation (2). These relations show a worse fit than the previous one (Table 5) due to higher dispersion in the experimental data, typical of fatigue behavior tests. The influence of the cutting parameters on the position of the fracture section, mainly at high *f* and $v_c$, should not be disregarded and their effect should be included in the equation.

**Table 9.** New equation coefficients.

| $v_c$ (m/min) | *f* (mm/rev) | Equation coefficients | | |
|---|---|---|---|---|
| | | C | α | $R^2$ |
| 40 | 0.05 | 511.62 | −0.052 | 0.82 |
| | 0.10 | 835.79 | −0.094 | 0.54 |
| | 0.15 | 826.56 | −0.094 | 0.44 |
| | 0.20 | 1195.30 | −0.130 | 0.54 |
| 60 | 0.05 | 1228.90 | −0.128 | 0.70 |
| | 0.10 | 467.48 | −0.049 | 0.50 |
| | 0.15 | 612.48 | −0.073 | 0.56 |
| | 0.20 | 837.63 | −0.099 | 0.57 |
| 80 | 0.05 | 981.74 | −0.108 | 0.65 |
| | 0.10 | 969.21 | −0.112 | 0.73 |
| | 0.15 | 1276.6 | −0.137 | 0.65 |
| | 0.20 | 1245.3 | −0.136 | 0.68 |

Considering these results, a new parametric relationship was proposed, according to Equation (3). Table 10 shows the values of C, x and y.

**Table 10.** Values of the constants for the marginal equation, $N = h(S,f)$, for the stress in the real fracture section.

| $v_c$ (m/min) | C | x | y | $R^2$ |
|---|---|---|---|---|
| 40 | $1.96 \times 10^{24}$ | −8.24 | −1.10 | 0.73 |
| 60 | $8.63 \times 10^{26}$ | −9.05 | −0.24 | 0.57 |
| 80 | $6.85 \times 10^{19}$ | −6.30 | −0.59 | 0.90 |

Compared to the previously obtained marginal equations, these new relations exhibited higher *f* dependence. The exponent for *f* (y) was higher in the whole range of the tested cutting speeds.

Even, this influence was significant for $v_c$ = 60 m/min, whereas it was negligible for the previous one. In addition, the difference with $S$ exponent (x) was lower. Hence, these equations fit better to reality and revealed higher influence of micro-geometrical deviations on fatigue behavior. Although the equations fit were slightly lower than the previous one, they show a reasonable fit, mainly for 40 and 80 m/min.

Figure 13 plots the parametrical potential equations exposed in Table 10. As previously commented, these relations show stronger dependence on $S$. Notwithstanding, the $f$ influence on $N$ was more noticeable at lower $S$ (200 MPa), especially for low $v_c$ (40 m/min), whereas $f$ exhibited lower influence at higher $S$.

Additionally, Figure 13 shows the $v_c$ influence on fatigue life ($N$). This influence was more noticeable in the low range of $S$ (200–250 MPa), and became less important above 250 MPa, regardless of $f$. As previously commented, this influence might be explained by considering that surface conditions take special importance in microcrack initiation at low $S$ values, being these surface conditions were related to the cutting parameters (mainly $f$). On the other hand, at higher values of $S$, surface conditions are less important, because microcrack initiation and nucleation quickly happen.

Finally, a potential parametric equation $N = g(S,v_c,f)$ was proposed, which includes the effect of $v_c$, as follows, according to Equation (4). Table 11 shows the results obtained for C, x, y and z.

**Table 11.** Values of the constants for the equation, $N = g(S,v_c,f)$, for the stress in the real fracture section.

| C | x | z | y | $R^2$ |
|---|---|---|---|---|
| $2.08 \times 10^{25}$ | −7.86 | −0.94 | −0.65 | 0.67 |

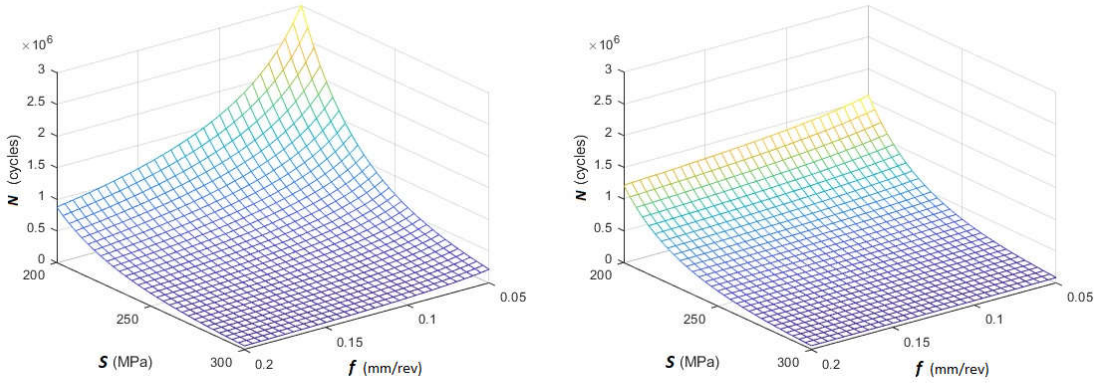


(**a**) (**b**)

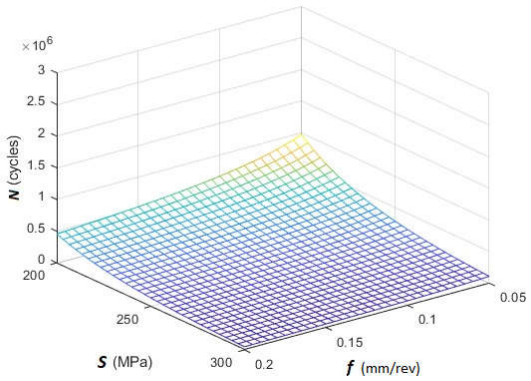

(**c**)

**Figure 13.** Potential relationships for $N = g(S,f)$, for the stress in the real fracture section: (**a**) $v_c$ = 40 m/min; (**b**) $v_c$ = 60 m/min and (**c**) $v_c$ = 80 m/min.

First, compared to the equation from Table 7, *S* influence was reduced and the influence of the cutting parameters ($v_c$, *f*) in fatigue behavior became more relevant, especially for *f*. This higher influence may be explained in part by the effect of macro-geometrical deviations on fatigue life. An *f* increase results in *CON* and *CYL* increments [56], regardless of *Ra*. Therefore, the influence of micro-geometrical deviations (and hence of *f*) on fatigue behavior is relevant, but the effect of *f* and $v_c$ on macro-geometrical deviations and these on fatigue behavior should not be neglected.

In addition, these new parameters for Equation (4) (Table 11) present the next advantages regarding the original coefficients (Table 7). On one hand, a better approximation to the roughness effect on *N* ($v_c$ = 60 m/min and *f* = 0.05 mm/rev, $v_c$ = 80 m/min and *f* = 0.15 mm/rev), showing the expected evolution of *N* as a function of *f* (close related with *Ra*). On the other hand, for $v_c$ = 60 and 80 m/min, at high *S* values, the cutting parameters influence was less significant, presenting $N = g(S,v_c,f)$ a greater convergence, as shown in Figure 12 b,c.

This equation allows predicting fatigue life as a function of the stress in the real fracture section (Wöhler curves) and corrects this value as a function of the input variables to the manufacturing process (cutting parameters, $v_c$ and *f*). The results from Table 11 show that, for the real fracture section position, also Equation (4) has shown a reasonable fit ($R^2$ = 0.67). For $v_c$ = 40 and 80 m/min, the corrected equation provides a good approximation for *N* ($R^2$ = 0.73 and 0.90 respectively, Table 10). Additionally, the equation fit for $v_c$ = 60 m/min was the lowest ($R^2$ = 0.57) and the dispersion of experimental results greater, within the common values for fatigue tests.

## 4. Conclusions

In this work, the influence of the cutting speed and feed on fatigue behavior of dry turning of the UNS A97075 (Al-Zn) alloy was analyzed. The study was performed using a rotating bar bending test with different applied loads. Additionally, the relative influence of micro and macro-geometrical deviations was discussed.

A general trend to increase *Ra* with *f* was observed, regardless of $v_c$. Therefore, *Ra* strongly depended on *f*, this cutting parameter being the most influential on micro-geometrical deviations, which is in good agreement with previous research.

Each tested value of *S*, $v_c$ and *f* modified the fatigue behavior of the specimens. In general, they negatively affected the fatigue life, reducing *N*. Regarding *f*, a general trend to decrease *N* with *f* was observed, regardless of $v_c$. This trend was more evident within the low range of load applied. An *f* increment resulted in higher *Ra* values, which made the crack initiation easier. Therefore, the surface topography was especially relevant in the crack initiation of fatigue failure at lower stresses and, as a result, *f* became more relevant. At higher stresses, this influence became lower and, therefore, surface roughness was less relevant. At high loads, other factors may be more prominent, such as the geometrical deviations, which are more influenced by the cutting speed.

With regard to $v_c$, a general trend to decrease *N* with $v_c$ was observed, regardless of *f*. In addition, the worst results were obtained when the highest *f* and $v_c$ were combined. An increase of $v_c$ resulted in an increment of geometrical deviations, which finally led to *N* reductions. Considering that $v_c$ had a very low influence on *Ra*, everything seemed to indicate that other variables (not only micro-geometrical deviations) took parts in the *S-N* evolution, especially for higher values of $v_c$ (residual stresses, microhardness and macro-geometrical deviations). This fact is relevant because, usually, the *S-N* curves were corrected only as a function of the micro-geometrical surface deviations and, hence, the effect of $v_c$ was usually neglected.

Several *S-N* parametric relations were proposed, for each cutting parameters combination. Furthermore, a potential parametric equation for $N = g(S,v_c,f)$ was proposed, which includes not only the effect of the stress on fatigue life but also the effect of the cutting speed and feed. This equation has shown a reasonable fit, taking in to account the usual dispersion in the fatigue test results, due to

the synergistic action of different factors, such as surface roughness, geometric deviations, residual stresses, surface microstructure changes or vibrations.

Additionally, the concentricity and cylindricity of the specimens were compared to the standard tolerance requirements. In most of the tests performed, the results were higher than those required in the standard. Hence, these macro-geometrical deviations may be an important factor to consider, mainly in the high range of the applied cutting parameters values. These high values for the macro-geometrical deviations resulted in the fracture of the specimen in a different area from that expected. Therefore, the stress values were recalculated as a function of the real position where fracture occurred and a new parametric equation for $N = g(S,v_c,f)$ was developed. This equation allows predicting fatigue life as a function of the stress in the real fracture section (Wöhler curves) and corrects this value as a function of the input variables to the manufacturing process (cutting parameters, $v_c$ and $f$), being these results are more conservative from a safety point of view.

These new relationships exhibited a lower dependence on $S$ and higher dependence on the cutting parameters and fit better to reality. An increase of $f$ resulted in *CON* and *CYL* increments, regardless of *Ra*. Therefore, the influence of micro-geometrical deviations (and hence of $f$) on fatigue behavior was relevant, but the effect of $f$ and $v_c$ on macro-geometrical deviations and these on fatigue behavior should not be neglected.

Finally, it is important to point out that the main objective of this work was not to get a complex model that explains the influence of machining on fatigue behavior from a physical point of view. The large number of variables involved in the process, interrelated to each other, makes it very difficult to obtain this kind of relations. However, a relationship between cutting parameters and fatigue behavior was obtained. This kind of analysis is highly demanded by the manufacturing industry, because it usually provides easy-to-apply equations that allow predicting the behavior of a process output variable based only on the input parameters. In addition, these equations facilitate the comprehension of the experimental results of this work.

It is necessary to highlight that the experimental results are valid within the range of the cutting parameters values tested and for this alloy. The generality of these parametric equations should be tested increasing the range of cutting speed and feed tested, including the cutting depth as well.

**Author Contributions:** S.M.B., F.J.T.V. and L.S.H. conceived and designed the experiments; S.M.B. performed the experiments; S.M.B., F.J.T.V., C.B.G. and L.S.H. analyzed the data; S.M.B. and F.J.T.V. wrote the paper; F.J.T.V., L.S.H. and C.B.G. revised the paper. All authors have read and agreed to the published version of the manuscript.

**Funding:** This research received no external funding.

**Acknowledgments:** The authors thank the University of Malaga-Andalucia Tech Campus of International Excellence for its economic contribution to this paper.

**Conflicts of Interest:** The authors declare that there is not conflict of interests regarding the publication of this paper.

## References

1. Gómez-Parra, A.; Álvarez-Alcón, M.; Salguero, J.; Batista, M.; Marcos, M. Analysis of the evolution of the Built-Up Edge and Built-Up Layer formation mechanisms in the dry turning of aeronautical aluminium alloys. *Wear* **2013**, *302*, 1209–1218.
2. Apostolos, F.; Alexios, P.; Georgios, P.; Panagiotis, S.; George, C. Energy Efficiency of Manufacturing Processes: A Critical Review. *Procedia CIRP* **2013**, *7*, 628–633.
3. Sheldon, R.A.; Green and sustainable manufacture of chemicals from biomass: State of the art. *Green Chem.* **2014**, *16*, 950–963.
4. Veleva, V.; Ellenbecker, M. Indicators of sustainable production: Framework and methodology. *J. Clean. Prod.* **2001**, *9*, 519–549.
5. Dornfeld, D. *Green Manufacturing: Fundamentals and Applications*; Springer: New York, NY, USA, 2013.
6. Alba-Galvín, J.; González-Rovira, L.; Bethencourt, M.; Botana, F.; Sánchez-Amaya, J. Influence of Aerospace Standard Surface Pretreatment on the Intermetallic Phases and CeCC of 2024-T3 Al-Cu Alloy. *Metals* **2019**, *9*, 320.

7. Wu, F.; Zhou, W.; Han, Y.; Fu, X.; Xu, Y.; Hou, H. Effect of Alloying Elements Gradient on Solid-State Diffusion Bonding between Aerospace Aluminum Alloys. *Materials* **2018**, *11*, 1446.
8. Trujillo, F.J.; Sevilla, L.; Marcos, M. Experimental parametric model for indirect adhesion wear measurement in the dry turning of UNS A97075 (Al-Zn) alloy. *Materials* **2017**, *10*, 152.
9. Batista, M.; Del Sol, I. Del; Gomez-Parra, A.; Ramirez-Peña, M.; Salguero, J. Study of the Tool Wear Process in the Dry Turning of Al–Cu Alloy. *Metals* **2019**, *9*, 1094.
10. Batista Ponce, M.; Del Sol Illana, I.; Fernandez-Vidal, S.; Salguero Gomez, J. Experimental Parametric Model for Adhesion Wear Measurements in the Dry Turning of an AA2024 Alloy. *Materials* **2018**, *11*, 1598.
11. Field, M.; Kahles, J.F.; Cammett, J.T. A review of measuring methods for surface integrity. *CIRP Ann. Manuf. Technol.* **1972**, *21*, 219–238.
12. Abrão, A.M.; Ribeiro, J.L.S.; Davim, J.P. Surface Integrity. In *Machining of Hard Materials*; Springer: London, UK, 2011; pp. 115–141.
13. Field, M.; Kahles, J.F.; Review of surface integrity of machined components. *Ann. CIRP* **1971**, *20*, 153–163.
14. M'Saoubi, R.; Outeiro, J.; Chandrasekaran, H.; Dillion, O.W., Jr.; Jawahir, I.S. A review of surface integrity in machining and its impact on functional performance and life of machined products. *Int. J. Sustain. Manuf.* **2008**, *1*, 203.
15. Koster, W.P.; Field, M.; Fritz, L.J.; Gatto, L.R.; Kahles, J.F.; *Surface Integrity of Machined Structural Components*; Air Force Systems Command, Air Force Materials Laboratory: Ohio, OH, USA, 1970.
16. Carpio, F.J.; Araújo, D.; Pacheco, F.J.; Méndez, D.; García, A.J.; Villar, M.P.; García, R.; Jiménez, D.; Rubio, L. Fatigue behaviour of laser machined 2024 T3 aeronautic aluminium alloy. *Appl. Surf. Sci*. **2003**, *208*, 194–198.
17. Matsumoto, Y.; Hashimoto, F.; Lahoti, G. Surface integrity generated by precision hard turning. *CIRP Ann. Manuf. Technol.* **1999**, *48*, 59–62.
18. Suraratchai, M.; Limido, J.; Mabru, C.; Chieragatti, R. Modelling the influence of machined surface roughness on the fatigue life of aluminium alloy. *Int. J. Fatigue* **2008**, *30*, 2119–2126.
19. Torres, A.; Puertas, I.; Luis, C.J. Surface roughness analysis on the dry turning of an Al-Cu alloy. *Procedia Eng*. **2015**, *132*, 537–544.
20. Trujillo, F.J.; Marcos Bárcena, M.; Sevilla, L. Experimental Prediction Model for Roughness in the Turning of UNS A97075 Alloys. *Mater. Sci. Forum* **2014**, *797*, 59–64.
21. Horváth, R.; Drégelyi-Kiss, Á. Analysis of surface roughness of aluminum alloys fine turned: United phenomenological models and multi-performance optimization. *Meas. J. Int. Meas. Confed.* **2015**, *65*, 181–192.
22. Rubio, E.M.; Camacho, A.M.; Sánchez-Sola, J.M.; Marcos, M. Surface roughness of AA7050 alloy turned bars: Analysis of the influence of the length of machining. *J. Mater. Process. Technol.* **2005**, *162*, 682–689.
23. Benardos, P.G.; Vosniakos, G.C.; Predicting surface roughness in machining: A review. *Int. J. Mach. Tools Manuf.* **2003**, *43*, 833–844.
24. Wiesner, C.; Künzi, H.U.; Ilschner, B. Characterization of the topography of turned surfaces and its influence on the fatigue life of Al-7075. *Mater. Sci. Eng. A* **1991**, *145*, 151–158.
25. Wojtowicz, N.; Danis, I.; Monies, F.; Lamesle, P.; Chieragati, R. The influence of cutting conditions on surface integrity of a wrought magnesium alloy. *Procedia Eng*. **2013**, *63*, 20–28.
26. Pawade, R.S.; Joshi, S.S.; Brahmankar, P.K. Effect of machining parameters and cutting edge geometry on surface integrity of high-speed turned Inconel 718. *Int. J. Mach. Tools Manuf.* **2008**, *48*, 15–28.
27. Arunachalam, R.M.; Mannan, M.A.; Spowage, A.C. Residual stress and surface roughness when facing age hardened Inconel 718 with CBN and ceramic cutting tools. *Int. J. Mach. Tools Manuf.* **2004**, *44*, 879–887.
28. Capello, E. Residual stresses in turning: Part I: Influence of process parameters. *J. Mater. Process. Technol.* **2005**, *160*, 221–228.
29. García Navas, V.; Gonzalo, O.; Bengoetxea, I. Effect of cutting parameters in the surface residual stresses generated by turning in AISI 4340 steel. *Int. J. Mach. Tools Manuf.* **2012**, 61, 48–57.
30. El-Helieby, S.O.A.; Rowe, G.W. Influences of surface roughness and residual stress on fatigue life of ground steel components. *Met. Technol.* **1980**, *7*, 221–225.
31. Reed, E.C.; Viens, J.A. The Influence of Surface Residual Stress on Fatigue Limit of Titanium. *J. Eng. Ind.* **1960**, *82*, 76.
32. Matsumoto, Y.; Magda, D.; Hoeppner, D.W.; Kim, T.Y. Effect of Machining Processes on the Fatigue Strength of Hardened AISI 4340 Steel. *J. Eng. Ind*. **1991**, *113*, 154.

33. Javidi, A.; Rieger, U.; Eichlseder, W. The effect of machining on the surface integrity and fatigue life. *Int. J. Fatigue* **2008**, *30*, 2050–2055.
34. Sun, J.; Wang, T.; Su, A.; Chen, W. Surface integrity and its influence on fatigue life when turning nickel alloy GH4169. *Procedia CIRP* **2018**, *71*, 478–483.
35. Gómez, A.; Sanz, A.; Marcos, M. An Analysis of the Influence of Cutting Parameters on the Turning Process on the Fatigue Life of Aluminum Alloy UNS A92024-T351. *Adv. Mater. Res.* **2012**, *498*, 19–24.
36. Rao, K.S.S.; Allamraju, K.V. Effect on Micro-Hardness and Residual Stress in CNC Turning of Aluminium 7075 Alloy. *Proc. Mater. Today* **2017**, *4*, 975–981.
37. Komanduri, R.; Hou, Z.B. A review of the experimental techniques for the measurement of heat and temperatures generated in some manufacturing processes and tribology. *Tribol. Int.* **2001**, *34*, 653–682.
38. Campbell, C.E.; Bendersky, L.A.; Boettinger, W.J.; Ivester, R. Microstructural characterization of Al-7075-T651 chips and work pieces produced by high-speed machining. *Mater. Sci. Eng. A* **2006**, *430*, 1–2, 15–26.
39. Rotella, G. Effect of surface integrity induced by machining on high cycle fatigue life of 7075-T6 aluminum alloy. *J. Manuf. Process.* **2019**, *41*, 83–91.
40. Zhenchao, Y.; Yang, X.; Yan, L.; Jin, X.; Quandai, W. The effect of milling parameters on surface integrity in high-speed milling of ultrahigh strength steel. *Proc. Procedia CIRP* **2018**, *71*, 83–88.
41. Srinivasa Rao, P.; Ramji, K.; Satyanarayana, B. Effect of wire EDM conditions on generation of residual stresses in machining of aluminum 2014 T6 alloy. *Alex. Eng. J.* **2016**, *55*, 1077–1084.
42. Jomaa, W.; Songmene, V.; Bocher, P. Surface Finish and Residual Stresses Induced by Orthogonal Dry Machining of AA7075-T651. *Materials* **2014**, *7*, 1603–1624.
43. Zhang, P.R.; Liu, Z.Q.; Guo, Y.B. Machinability for dry turning of laser cladded parts with conventional vs. wiper insert. *J. Manuf. Process.***2017**, *28*, 494–499.
44. Sugihara, T.; Singh, P.; Enomoto, T. Development of novel cutting tools with dimple textured surfaces for dry machining of aluminum alloys. *Procedia Manuf.* **2017**, *14*, 111–117.
45. Shigley, J.E.; Mischke, C.R.; Budynas, R.G. *Mechanical Engineering Design*; Mc Graw Hill: New York, NY, USA, 2007.
46. International Organization for Standardization. *ISO 1143:2010 Metallic Materials — Rotating bar Bending Fatigue Testing*; International Organization for Standardization: Geneva, Switzerland, 2010.
47. Díaz, M.S.; Gil, M.J. Á.; MacHuca, J.A.D. Performance measurement systems, competitive priorities, and advanced manufacturing technology: Some evidence from the aeronautical sector. *Int. J. Oper. Prod. Manag.* **2005**, *25*, 781–799.
48. International Organization for Standardization. I*SO 1099:2017 Metallic Materials — Fatigue Testing — Axial Force-Controlled Method*; International Organization for Standardization: Geneva, Switzerland, 2017.
49. International Organization for Standardization. *ISO 1352:2011 Metallic Materials — Torque-Controlled Fatigue Testing*; International Organization for Standardization: Geneva, Switzerland, 2011.
50. International Organization for Standardization. *ISO 12106:2017 Metallic Materials — Fatigue Testing — Axial-Strain-Controlled Method*; International Organization for Standardization: Geneva, Switzerland, 2017.
51. Smojver, I.; Ivančević, D. Application of Numerical Methods in the Improvement of Safety of Aeronautical Structures. *Transp. Res. Procedia* **2017**, *28*, 164–172.
52. Goncharenko, A.V. Aeronautical and Aerospace Material and Structural Damages to Failures: Theoretical Concepts. *Int. J. Aerosp. Eng.* **2018**, *2018*.
53. Trujillo Vilches, F.J.; Martín-Béjar, S.; Bermudo Gamboa, C.; Sevilla Hurtado, L. *Fatigue Test Bench Manufacturing by Reusing a Parallel Lathe*; Advances in Manufacturing Technology XXXII: Skovde, Sweden, 2018; pp. 15–20.
54. Trujillo, F.J.; Sevilla, L.; Salguero, J.; Batista, M.; Marcos, M. Parametric potential model for determining the micro-geometrical deviations of horizontally dry-turned UNS A97075 (Al-Zn) alloy. *Advanced Science Letters* **2013**, *13*, 731-735.
55. Martín-Béjar, S.; Trujillo Vilches, F.J.; Bermudo Gamboa, C.; Sevilla Hurtado, L. Cutting Speed and Feed Influence on Surface Microhardness of Dry-Turned UNS A97075-T6 Alloy. *Appl. Sci.* **2020**, *10*, 1049.
56. Martín Béjar, S.; Trujillo Vilches, F.J.; Bermudo Gamboa, C.; Sevilla Hurtado, L. Parametric analysis of macro-geometrical deviations in dry turning of UNS A97075 (Al-Zn) alloy. *Metals* **2019**, *9*, 11.

57. International Organization for Standardization. *ISO 12107:2012. Metallic Materials—Fatigue Testing—Statistical Planning and Analysis of Data*; International Organization for Standardization: Geneva, Switzerland, 2012.
58. Schijve, J. *Fatigue of Structures and Materials*; Springer: Dordrecht, The Netherlands, 2009.
59. Singh, A.K.; Datta, S.; Chattopadhyay, A.; Riddick, J.C.; Hall, A.J. Fatigue crack initiation and propagation behavior in Al—7075 alloy under in-phase bending-torsion loading. *Int. J. Fatigue* **2019**, *126*, 346–356.
60. Puchi-Cabrera, E.S.; Staia, M.H.; Santana, Y.Y.; Mora, E.J.; Lesage, J.; Chicot, D.; La barbera, J.G.; Ochoa, E.; Villalobos, C.J. Fatigue behavior of AA7075-T6 aluminum alloy coated with a WC-10Co-4Cr cermet by HVOF thermal spray. *Surf. Coat. Technol.* **2013**, *220*, 122–130.